Chapter

Power Converter Topologies for Multiphase Drive Applications

Carlos A. Reusser

Abstract

The yet growing demand for higher demanding industrial applications and the global concern about harmful emissions in the atmosphere have increased the interest for new developments in electric machines and power converters. To meet these new requirements, multiphase machines have become a very attractive solution, offering potential advantages over three-phase classical solutions. Multiphase machine's power demand can be split over more than three phases, thus reducing the electric field stress on each winding (protecting the insulation system) and the requirements on maximum power ratings, for semiconductor devices. Moreover, only two degrees of freedom (i.e. two independently controllable currents) are required for independent flux and torque control. Due to the previous facts, the use of multiphase drives has become very attractive for applications and developments in areas such as electric ship propulsion, more-electric aircraft, electric and hybrid electric road vehicles, electric locomotive traction and in renewable electric energy generation. As a consequence of this multiphase drive tendency, the development of power converter topologies, capable of dealing with high power ratings and handling multiphase winding distributions, has encourage the development of new converter topologies, control strategies and mathematical tools, to face this new challenge.

Keywords: multiphase AC drive, neutral-point clamped, cascaded H-bridge, nine-switch converter, 11-switch converter, field-oriented control (FOC), direct torque control (DTC)

1. Introduction

Multiphase variable-speed drives, based on multiphase AC machines, are nowadays the most natural solution for high-demanding industrial, traction and power generation and distribution applications [1].

The types of multiphase machines for variable-speed applications are in principle the same as their three-phase counterparts. These are synchronous machines, which depending on the excitation can be subclassified into wound rotor, permanent magnet or reluctance machines and induction machines.

In a multiphase winding, the stator winding distribution becomes more concentrated, rather than distributed, as in the case of three-phase windings. This fact and the particularity of using quasi-sinusoidal, rather than sinusoidal voltages because of the inverting process in the power conversion stage, have several advantages that can be summarized as lower field harmonics content and better fault tolerance, because of extra degrees of freedom and less susceptibility to torque pulsations, due to an excitation field with less harmonic content [2].

As a consequence, the use of a multiphase winding configuration improves the MMF spatial distribution, by reducing its harmonic content and losses, due to flux leakage, and increasing the machine's efficiency. These facts have increased the interest for research and development for transportation applications, such as cargo ships, aircraft and road vehicles, thus also contributing to the reduction of greenhouse effect emissions.

2. Mathematical modeling of multiphase machines

All electrical machines can be found to be variations of a common set of fundamental principles, which apply alike the number of phases of which the machine is constructed.

In this context, multiphase machines can be treated as belonging to an n-dimensional space, corresponding to the respective state variables. The machine model, on its original phase-variable form, can be transformed into $n/2$ two-dimensional subspaces, for a machine with an even number of phases. If the number of phases is odd, then the original n-dimensional subspace can be decomposed into a $(n-1)/2$ two-dimensional subspaces and a single-dimensional quantity, which corresponds to a common mode subspace.

Each new two-dimensional subspace is orthogonal to each other, so there is no mutual coupling and they are represented in a stationary reference frame, respecting all other state variables. These new two-dimensional subspaces are could be denoted as $u_k v_k$, where k stands for the respective new orthogonal subspace.

Let us consider an arbitrary state variable λ, defined as $\boldsymbol{\lambda} = [\lambda_1 \lambda_2 \ldots \lambda_n]^T$, and let $T\langle\,\rangle$ be a linear operator, which transforms the n-dimensional space into $n/2$ two-dimensional subspaces, for n even, as in Eq. (1):

$$T\langle\,\rangle = \sqrt{\frac{2}{n}}\begin{bmatrix} 1 & \cos(\alpha) & \cos(2\alpha) & \ldots & \cos(2\alpha) & \cos(\alpha) \\ 0 & \sin(\alpha) & \sin(2\alpha) & \ldots & -\sin(2\alpha) & -\sin(\alpha) \\ 1 & \cos(2\alpha) & \cos(4\alpha) & \ldots & \cos(4\alpha) & \cos(2\alpha) \\ 0 & \sin(2\alpha) & \sin(4\alpha) & \ldots & -\sin(4\alpha) & -\sin(2\alpha) \\ \vdots & \vdots & \vdots & \vdots & \vdots & \vdots \\ 1 & \cos\left(\frac{n}{2}\right)\alpha & \cos 2\left(\frac{n}{2}\right)\alpha & \ldots & \cos 2\left(\frac{n}{2}\right)\alpha & \cos\left(\frac{n}{2}\alpha\right) \\ 0 & \sin\left(\frac{n}{2}\right)\alpha & \sin 2\left(\frac{n}{2}\right)\alpha & \ldots & -\sin 2\left(\frac{n}{2}\right)\alpha & -\sin\left(\frac{n}{2}\right)\alpha \end{bmatrix} \tag{1}$$

In the case of n odd, then the corresponding transformation is given as in Eq. (2):

$$T\langle\,\rangle = \sqrt{\frac{2}{n}}\begin{bmatrix} 1 & \cos(\alpha) & \cos(2\alpha) & \cdots & \cos(2\alpha) & \cos(\alpha) \\ 0 & \sin(\alpha) & \sin(2\alpha) & \cdots & -\sin(2\alpha) & -\sin(\alpha) \\ 1 & \cos(2\alpha) & \cos(4\alpha) & \cdots & \cos(4\alpha) & \cos(2\alpha) \\ 0 & \sin(2\alpha) & \sin(4\alpha) & \cdots & -\sin(4\alpha) & -\sin(2\alpha) \\ \vdots & \vdots & \vdots & \vdots & \vdots & \vdots \\ 1 & \cos\left(\frac{(n-1)}{2}\right)\alpha & \cos 2\left(\frac{(n-1)}{2}\right)\alpha & \cdots & \cos 2\left(\frac{(n-1)}{2}\right)\alpha & \cos 2\left(\frac{(n-1)}{2}\right)\alpha \\ 0 & \sin\left(\frac{(n-1)}{2}\right)\alpha & \sin 2\left(\frac{(n-1)}{2}\right)\alpha & \cdots & -\sin 2\left(\frac{(n-1)}{2}\right)\alpha & -\sin 2\left(\frac{(n-1)}{2}\right)\alpha \\ \sqrt{\frac{1}{2}} & \sqrt{\frac{1}{2}} & \sqrt{\frac{1}{2}} & \cdots & \sqrt{\frac{1}{2}} & \sqrt{\frac{1}{2}} \end{bmatrix} \tag{2}$$

The last row of $T\langle\,\rangle$ in Eq. (2) corresponds to the projection of the state variable onto the common mode subspace.

Using the above-presented mathematical decomposition, any machine can be represented by an equivalent two-axis idealized machine, called the Kron's primitive machine. The Kron's primitive machine corresponds to the representation of the n-dimensional space, in the u_1v_1 or $\alpha\beta$ subspace, using the linear transformation $T\langle\,\rangle_{n\to\alpha\beta}$; this definition can be found as the generalized theory of electrical machines.

The mathematical model describing a generalized n-dimensional electrical machine is given in Eqs. (3) and (4), for dynamics, respectively:

$$\boldsymbol{v_s} = [R_s]\,\boldsymbol{i_s} + \frac{d}{dt}\boldsymbol{\psi_s} \tag{3}$$

$$\boldsymbol{v_r} = [R_r]\,\boldsymbol{i_r} + \frac{d}{dt}\boldsymbol{\psi_r} \tag{4}$$

$$\boldsymbol{v_s} = [v_{s1}v_{s2}\ldots v_{sn}]^T \qquad \boldsymbol{i_s} = [i_{s1}i_{s2}\ldots i_{sn}]^T \qquad \boldsymbol{\psi_s} = [\psi_{s1}\psi_{s2}\ldots\psi_{sn}]^T \tag{5}$$

$$\boldsymbol{v_r} = [v_{r1}v_{r2}\ldots v_{rn}]^T \qquad \boldsymbol{i_r} = [i_{r1}i_{r2}\ldots i_{rn}]^T \qquad \boldsymbol{\psi_r} = [\psi_{r1}\psi_{r2}\ldots\psi_{rn}]^T \tag{6}$$

Considering symmetrical windings for both stator and rotor, then $[R_s]$ and $[R_r]$ are diagonal $n \times n$ matrices, thus $[R_s] = diag\,(R_s)^{(n)}$ and $[R_r] = diag\,(R_r)^{(n)}$. The stator and rotor flux linkages can be found as in Eqs. (7) and (8):

$$\boldsymbol{\psi_s} = [L_s]\,\boldsymbol{i_s} + [L_{sr}]\,\boldsymbol{i_r} \tag{7}$$

$$\boldsymbol{\psi_r} = [L_r]\,\boldsymbol{i_r} + [L_{rs}]\,\boldsymbol{i_s} \tag{8}$$

where due to the machine's symmetry $[L_{rs}] = [L_{sr}]^T$; the corresponding stator and rotor inductance matrices are described as follows:

$$[L_s] = \begin{bmatrix} L_{s11} & L_{s12} & \ldots & L_{s1(n-1)} & L_{s1n} \\ \vdots & \vdots & \vdots & \vdots & \vdots \\ L_{sn1} & L_{sn2} & \ldots & L_{sn(n-1)} & L_{snn} \end{bmatrix} \tag{9}$$

$$[L_r] = \begin{bmatrix} L_{r11} & L_{r12} & \ldots & L_{r1(n-1)} & L_{r1n} \\ \vdots & \vdots & \vdots & \vdots & \vdots \\ L_{rn1} & L_{rn2} & \ldots & L_{rn(n-1)} & L_{rnn} \end{bmatrix} \tag{10}$$

It has to be noticed that for both stator and rotor windings, $L_{11} = L_{22} = \ldots = L_{nn}$ which correspond to the winding self-inductance $\overline{L}$; for the corresponding stator and rotor self-inductances within each one, due to the machine's symmetry, it fulfills that $L_{jk} = L_{kj} = L_m \quad \forall j,k\; j \neq k$. Then for the stator and rotor winding self-inductances, it can be stated that $L_{jj} = L_\sigma + L_m$ where L_σ corresponds to the stator or rotor winding leakage inductance. On the other hand, the stator-to-rotor mutual inductance matrix $[L_{sr}]$ can be found as in Eq. (11):

$$[L_{sr}] = M\begin{bmatrix} \cos(\theta_r) & \cos(\theta_r-(n-1)\alpha) & \cos(\theta_r-(n-2)\alpha) & \ldots & \cos(\theta_r-\alpha) \\ \cos(\theta_r-\alpha) & \cos(\theta_r) & \cos(\theta_r-(n-1)\alpha) & \ldots & \cos(\theta_r-2\alpha) \\ \cos(\theta_r-2\alpha) & \cos(\theta_r-\alpha) & \cos(\theta_r) & \ldots & \cos(\theta_r-3\alpha) \\ \vdots & \vdots & \vdots & \ldots & \vdots \\ \cos(\theta_r-(n-1)\alpha) & \cos(\theta_r-(n-2)\alpha) & \cos(\theta_r-(n-3)\alpha) & \ldots & \cos(\theta_r) \end{bmatrix} \tag{11}$$

The resulting generalized machine representation is obtained by applying the linear transformation operator $T\langle\,\rangle_{n\to\alpha\beta}$ to Eqs. (3) and (4), resulting in the following dynamic representation, in the $\alpha\beta$ subspace, in Eqs. (12) and (13):

$$\boldsymbol{v}_s^{(\alpha\beta)} = R_s\,\boldsymbol{i}_s^{(\alpha\beta)} + \frac{d}{dt}\,\boldsymbol{\psi}_s^{(\alpha\beta)} \tag{12}$$

$$\boldsymbol{v}_r^{(\alpha\beta)} = R_s\,\boldsymbol{i}_r^{(\alpha\beta)} + \frac{d}{dt}\,\boldsymbol{\psi}_r^{(\alpha\beta)} - j\,\omega_r\boldsymbol{\psi}_r^{(\alpha\beta)} \tag{13}$$

The corresponding stator and rotor flux linkages given in Eqs. (7) and (8) are transformed into the $\alpha\beta$ subspace as in Eqs. (14) and (15):

$$\boldsymbol{\psi}_s^{(\alpha\beta)} = [L_s]\,\boldsymbol{\psi}_s^{(\alpha\beta)} + [L_{sr}]\,\boldsymbol{i}_r^{(\alpha\beta)} \tag{14}$$

$$\boldsymbol{\psi}_r^{(\alpha\beta)} = [L_r]\,\boldsymbol{i}_r^{(\alpha\beta)} + [L_{rs}]\,\boldsymbol{i}_s^{(\alpha\beta)} \tag{15}$$

The presented methodology considers a n-phase winding with uniform distribution that is $\alpha = \frac{2\pi}{n}$; in the case of machine with multiple groups of three-phase windings, α is the shifting angle between each group of three-phase windings. It has to be noted that for each three-phase winding transformation, an additional row has to be included in Eq. (2).

The developed electromechanical torque can be expressed in terms of the electromechanical energy conversion as in Eqs. (16) and (17):

$$T_e = \frac{\partial}{\partial\theta_r}\,W_{fld}\left(\boldsymbol{i}_s^{(\alpha\beta)}, \boldsymbol{\psi}_s^{(\alpha\beta)}, \theta_r\right) \tag{16}$$

$$T_e = \frac{1}{2}\left[\boldsymbol{i}^{(\alpha\beta)}\right]\frac{\partial}{\partial\theta_r}\,[L]\left[\boldsymbol{i}^{(\alpha\beta)}\right]^T \tag{17}$$

$$\left[\boldsymbol{i}^{(\alpha\beta)}\right] = \begin{bmatrix}\boldsymbol{i}_s^{(\alpha\beta)} & \boldsymbol{i}_r^{(\alpha\beta)}\end{bmatrix}^T \tag{18}$$

$$[L] = \begin{bmatrix}[L_s] & [L_{sr}] \\ [L_{sr}]^T & [L_r]\end{bmatrix} \tag{19}$$

Following the electromechanical torque can be expressed as in Eq. (20):

$$T_e = \frac{1}{2}\,\boldsymbol{i}_s^{(\alpha\beta)}\,\frac{\partial}{\partial\theta_r}\,[L_{sr}]\,\boldsymbol{i}_r^{(\alpha\beta)^T} \tag{20}$$

The generalized machine representation given by Eqs. (12), (13) and (20) can be expressed in an arbitrary orthogonal synchronous reference frame dq, which rotates at synchronous speed ω_k; thus the corresponding rotation into the dq state variables is given by Eq. (21):

$$\theta_k = \int \omega_k\,dt \tag{21}$$

Rotation into the dq subspace is given by the unitary rotation matrix U defined in Eq. (22):

$$U = \begin{bmatrix}\cos\theta_k & \sin\theta_k \\ -\sin\theta_k & \cos\theta_k\end{bmatrix} \tag{22}$$

The generalized machine dynamic representation in the dq reference frame, as consequence of the rotation of Eqs. (12), (13) and (20), is given in Eqs. (23)–(25),

representing the Kron's primitive machine model in a generalized synchronous reference frame:

$$\boldsymbol{v}_s^{(dq)} = R_s \boldsymbol{i}_s^{(dq)} + \frac{d}{dt}\boldsymbol{\psi}_s^{(dq)} + j\omega_k \boldsymbol{\psi}_s^{(dq)} \tag{23}$$

$$\boldsymbol{v}_r^{(dq)} = R_s \boldsymbol{i}_r^{(dq)} + \frac{d}{dt}\boldsymbol{\psi}_r^{(dq)} + j(\omega_k - \omega_r)\boldsymbol{\psi}_r^{(dq)} \tag{24}$$

$$T_e = p\frac{L_m}{L_r}\left(\psi_r^d i_s^q - \psi_r^q i_s^d\right) \tag{25}$$

Equations (23) and (24) can be written in their matrix form as in Eq. (26), becoming a generalized impedance model, as described in Eq. (27):

$$\begin{bmatrix} v_s^d \\ v_s^q \\ v_r^d \\ v_r^q \end{bmatrix} = \begin{bmatrix} R_s + L_s\frac{d}{dt} & -\omega_k L_s & L_m\frac{d}{dt} & -\omega_k L_m \\ \omega_k L_s & R_s + L_s\frac{d}{dt} & \omega_k L_m & L_m\frac{d}{dt} \\ L_m\frac{d}{dt} & -(\omega_k - \omega_r)L_m & R_r + L_r\frac{d}{dt} & -(\omega_k - \omega_r)L_r \\ (\omega_k - \omega_r)L_m & L_m\frac{d}{dt} & (\omega_k - \omega_r)L_r & R_r + L_r\frac{d}{dt} \end{bmatrix} \begin{bmatrix} i_s^d \\ i_s^q \\ i_r^d \\ i_r^q \end{bmatrix} \tag{26}$$

$$\left[\boldsymbol{v}^{(dq)}\right] = [z]\left[\boldsymbol{i}^{(dq)}\right] \tag{27}$$

2.1 Multiphase synchronous machines

The use of multiphase synchronous machines has been focused on its application for medium- and high-power generation systems, being their primary use, on wind energy conversion systems (WECS). The previous statement is based on the fact that most of wind energy conversion systems operate in the low-voltage range, principally due to restrictions of winding insulation. This fact has stimulated the development of multiphase generator topologies, thus gaining increasing interest in the research for new converter topologies [3, 4]. Some of their main advantages are the following:

- The total power can be divided into lower power converters.
- Due to that each converter is insulated from each other, there is no circulating current between converters, which leads to no power derating for the converters.
- The increase of the number of phases in the generator voltages is phase-shifted so that low-order harmonics are reduced and consequently smaller filters can be used.
- Reduced torque pulsations.
- Fault-tolerant redundancy under winding fault conditions.
- Additional degrees of freedom which can be used to improve the machine performance.

Arrangement of multiple three-phase windings has become a very popular construction technique, for multiphase machines. In this field, the most common

configuration is the six-phase machine, based on two independent three-phase windings, which are spatially shifted in 30 degrees, as shown in **Figure 1**.

The use of multiple three-phase windings has the advantage of guaranteeing full decoupling under faulty conditions, thus preventing the circulation of common mode currents and pulsating torque.

The linear transformation operator $T\langle\,\rangle$ is defined as in Eq. (28), with $\varphi = \frac{\pi}{6}$:

$$T\langle\,\rangle = \frac{1}{\sqrt{3}}\begin{bmatrix} 1 & \cos 4\varphi & \cos 8\varphi & \cos\varphi & \cos 5\varphi & \cos 9\varphi \\ 0 & \sin 4\varphi & \sin 8\varphi & \sin\varphi & \sin 5\varphi & \sin 9\varphi \\ 1 & \cos 8\varphi & \cos 4\varphi & \cos 5\varphi & \cos\varphi & \cos 9\varphi \\ 0 & \sin 8\varphi & \sin 4\varphi & \sin 5\varphi & \sin\varphi & \sin 9\varphi \\ 1 & 1 & 1 & 0 & 0 & 0 \\ 0 & 0 & 0 & 1 & 1 & 1 \end{bmatrix} \tag{28}$$

The equivalent model in the dq synchronous subspace can be derived from Eq. (26); in this case it has to be noted that the synchronous reference frame dq coincides with the rotor natural reference frame, thus $\omega_k = \omega_r$, becoming Eq. (29) and (30) for the stator:

$$v_s^d = R_s i_s^d + \frac{d}{dt}\psi_s^d - \omega_k \psi_s^q \tag{29}$$

$$v_s^q = R_s i_s^q + \frac{d}{dt}\psi_s^q + \omega_k \psi_s^d \tag{30}$$

Equations (31) and (32) correspond to the damping winding effect:

$$0 = R_r i_r^d + \frac{d}{dt}\psi_r^d \tag{31}$$

$$0 = R_r i_r^q + \frac{d}{dt}\psi_r^q \tag{32}$$

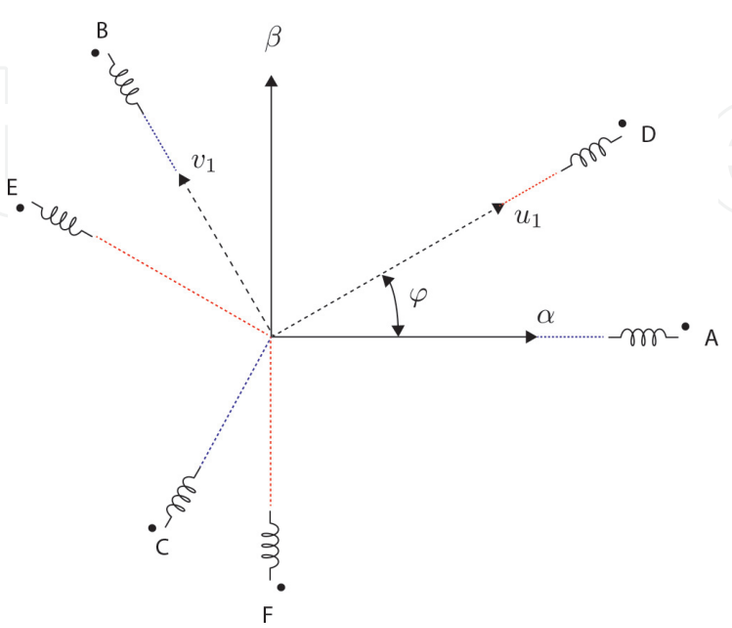

Figure 1.
Dual three-phase stator winding configuration.

The corresponding flux linkages, considering the general case of an anisotropic machine, are given in the following equations:

$$\psi_s^d = L_{sd} i_s^d + L_{md} i_r^d + \psi_m \tag{33}$$

$$\psi_s^q = L_{sq} i_s^q + L_{mq} i_r^q \tag{34}$$

$$\psi_r^d = L_{rd} i_r^d + L_{md} i_s^d + \psi_m \tag{35}$$

$$\psi_r^q = L_{rq} i_r^q + L_{mq} i_s^q \tag{36}$$

and the electromechanical torque is given in Eq. (37):

$$T_e = p\left[\psi_m i_s^q + \left(L_{md} i_r^d i_s^q - L_{mq} i_r^q i_s^d\right)\right] + p\left[L_{md} - L_{mq}\right] i_s^q i_s^d \tag{37}$$

2.2 Multiphase induction machines

Modern industrial high-demanding processes are commonly based on induction machines. They are very attractive for these kind of applications because of their simplicity and capability to work under extreme torque demanding conditions [5].

Within the previous context, multiphase induction machines have become very popular for applications where high redundancy and power density are required. In particular, the use of multiple three-phase windings (six and nine phases) in naval propulsion systems has aroused much interest and encouraged the research of new multiphase converter topologies and control schemes [6, 7].

Based on the Kron's primitive machine model developed in Eq. (26), the dynamical model of the multiphase induction machine is given in Eqs. (38)–(41):

$$v_s^d = R_s i_s^d + \frac{d}{dt}\psi_s^d - \omega_k \psi_s^q \tag{38}$$

$$v_s^q = R_s i_s^q + \frac{d}{dt}\psi_s^q + \omega_k \psi_s^d \tag{39}$$

$$0 = R_r i_r^d + \frac{d}{dt}\psi_r^d \tag{40}$$

$$0 = R_r i_r^q + \frac{d}{dt}\psi_r^q \tag{41}$$

Due to the isotropy of the induction machine and the absence of an MMF source in the rotor (permanent magnets or field winding), the corresponding flux linkages are given in Eqs. (42)–(45):

$$\psi_s^d = L_s i_s^d + L_m i_r^d \tag{42}$$

$$\psi_s^q = L_s i_s^q + L_m i_r^q \tag{43}$$

$$\psi_r^d = L_r i_r^d + L_m i_s^d \tag{44}$$

$$\psi_r^q = L_r i_r^q + L_m i_s^q \tag{45}$$

The electromechanical torque expression can be derived from Eq. (37) by considering $\psi_m = 0, L_{md} = L_{mq} = L_m$, becoming Eq. (46):

$$T_e = p L_m \left[i_r^d i_s^q - i_r^q i_s^d\right] \tag{46}$$

3. Multiphase power converters

As stated previously, multiphase machines have many advantages over traditional three-phase-based machine drives, by reducing the impact of low-frequency torque pulsations and the dc-link current harmonic content. They also, due to the nature of their winding configuration, improve the system reliability, by introducing redundant operation conditions. As a consequence the use of multiphase converter topologies with multiphase drive arrangements has been proved as a viable approach for its application in high-demanding industrial applications.

In this field, the development of power converters capable to deal with the multiphase machine structure has capture much attention in the recent years; thus several topologies have been introduced in the last decades. This topologies can consist of arrangements of conventional two-level three-phase voltage source converters (2LVSC), multilevel converters (MLVSC) or in more specialized and dedicated topologies such as multiphase matrix converters.

3.1 Classical topologies

Classical topologies for multiphase converters are commonly based in arrangements of parallel-connected fundamental cells (multiple legs), or in multiple channel configuration, of voltage source converter topologies.

Commonly used topologies for multiphase applications are H-bridge converter (HBC), neutral-point clamped converter (NPC) and the cascaded H-bridge (CHB) topology, which are shown in **Figure 2**.

Classical multiphase VSC topologies consist of an arrangement of n individual half-cells connected in parallel to a single dc-link, as shown in **Figure 3**.

Modulation of each individual half-cell circuit is implemented in such a way, to obtain n voltage output signals shifted by $2\pi/n$. Generation of the required voltage signals is supported by classical carrier-based strategies, such as sinusoidal pulse width modulation (SPWM) and space vector pulse width modulation (SVPWM).

SPWM methods can be implemented for two-level or multilevel half-cells. In the first case, only one high-frequency carrier is required for the respective switching signals per phase S_x, as given in Eqs. (46) and (48):

$$S_x = \begin{cases} 1 & |u^*_{xN}| \geq |u_c| \\ 0 & |u^*_{xN}| < |u_c| \end{cases} \tag{47}$$

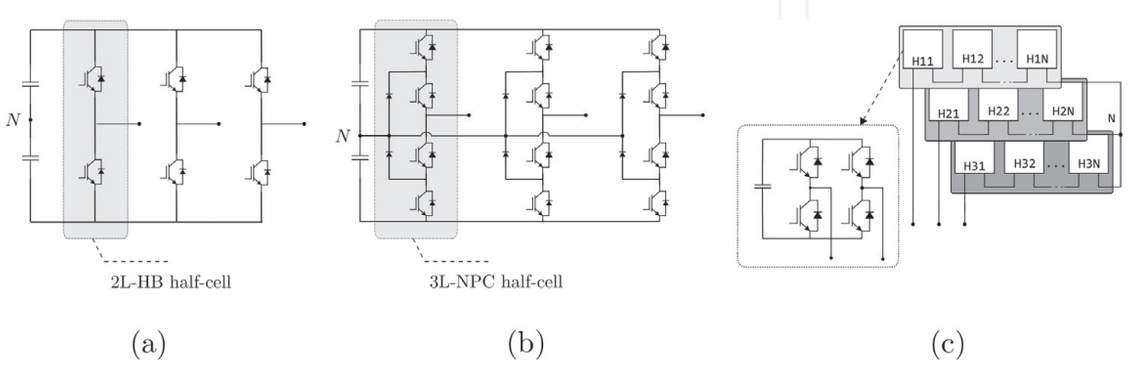

Figure 2.
Classical VSC topologies: (a) two-level bridge, (b) neutral-point clamped and (c) cascaded H-bridge.

$$u_{xN}^{*} = v_{xN}^{*} - \frac{1}{2}\left\{min\left(v_{aN}^{*}, v_{bN}^{*}, \ldots, v_{nN}^{*}\right) + max\left(v_{aN}^{*}, v_{bN}^{*}, \ldots, v_{nN}^{*}\right)\right\} \tag{48}$$

where x stands for the corresponding phase $x = [1, \ldots, n]$, u_{xN}^{*} is the reference to be synthesized for the corresponding phase, and u_c stands for the carrier wave.

For multilevel parallel arrangements (NPC or CHB), the use of multiple carries, as an extension of the two-level PWM methods, has been proven as a suitable solution. Level-shifted PWM (LSPWM) has become a very popular modulation technique, because it fits for any multilevel converter topology and ensures low harmonic distortion. The corresponding switching states are given in Eq. (49):

$$S_{xm} = \begin{cases} 1 & |u_{xN}^{*}| \geq |u_{cm}| \\ 0 & |u_{xN}^{*}| < |u_{cm}| \end{cases} \tag{49}$$

where x stands for the corresponding phase $x = [1, \ldots, n]$, m to the corresponding level and, u_{cm} is the carrier for the matched m level.

The main advantages of this topology are its simplicity by using half-bridges for each leg (phase), and the requirement of a single dc-link the feed the n-phase inverting stage. The use of a parallel arrangement of fundamental half-cells generates $(n-1)$ dimensional spaces, which can be decomposed into $(n-1)/2$ subspaces, ensuring redundant switching states.

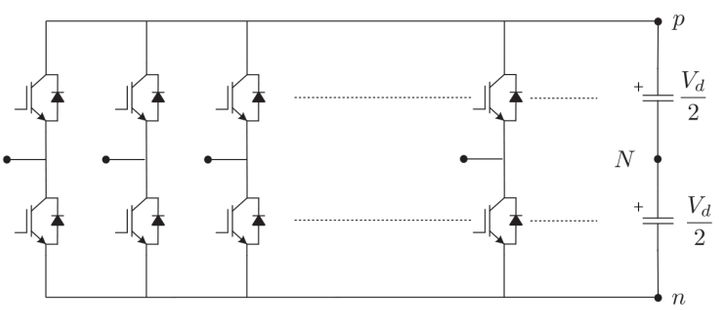

Figure 3.
Multiphase multicell topology.

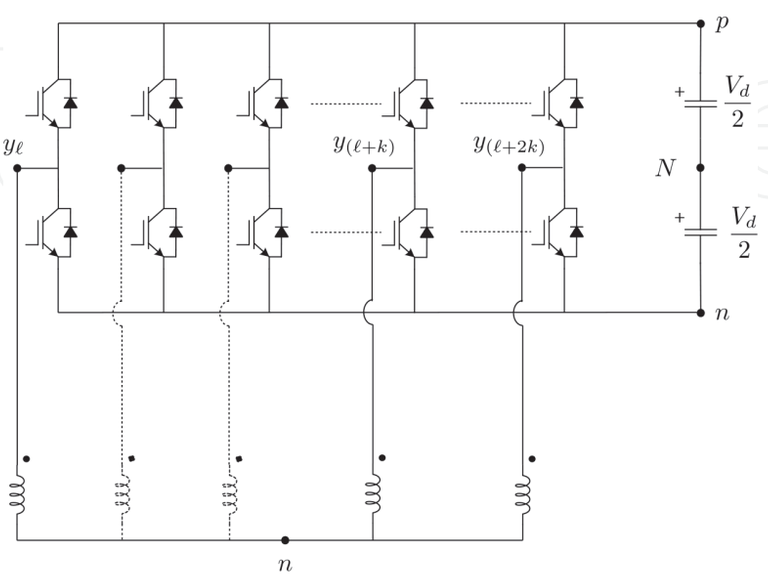

Figure 4.
Common connected load arrangement.

Multicell topology also enables the possibility to have common or split connected loads. In the first case, each phase in the load side is connected to a common neutral point N as presented in **Figure 4**; the main drawback with this configuration is the circulation of zero sequence currents, since the neutral points $N - n$ are not insulated, thus establishing a common mode voltage $v_{Nn} \neq 0$ in the dq synchronous reference frame.

Split connected load arrangement is possible, if $n = 3k|k = [1, 2, \ldots]$, so the n phase system can be divided into k three-phase insulated independent subsystems, as shown in **Figure 5**, with symmetric or asymmetric electrical shifting δ. It has to be noted that independently on the symmetric or asymmetric configuration, the

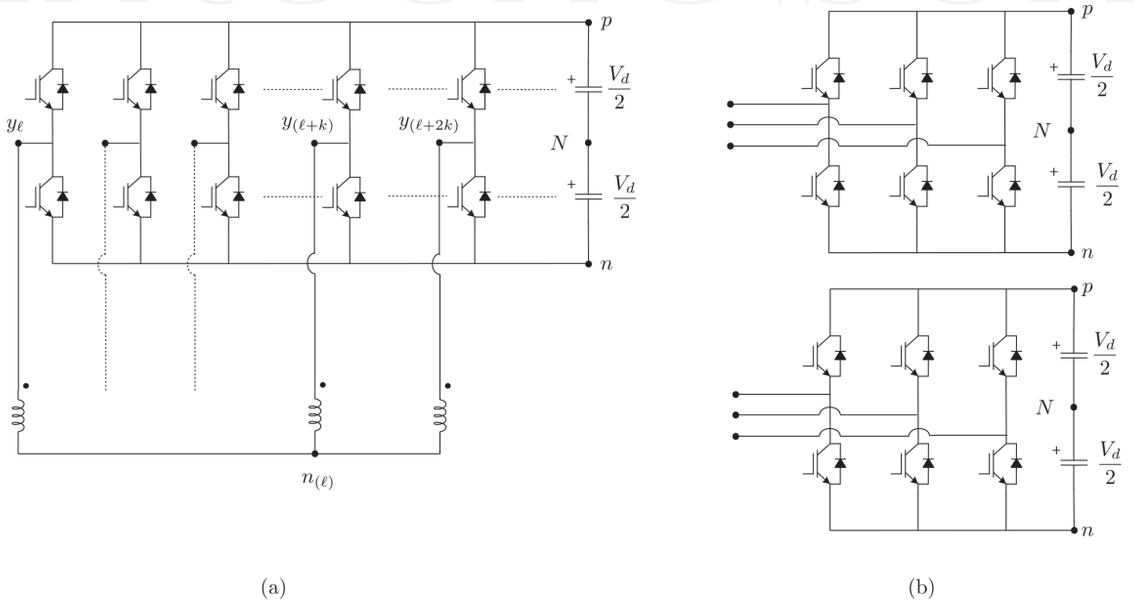

Figure 5.
Split connected load arrangements. (a) Single-channel topology and (b) multichannel topology.

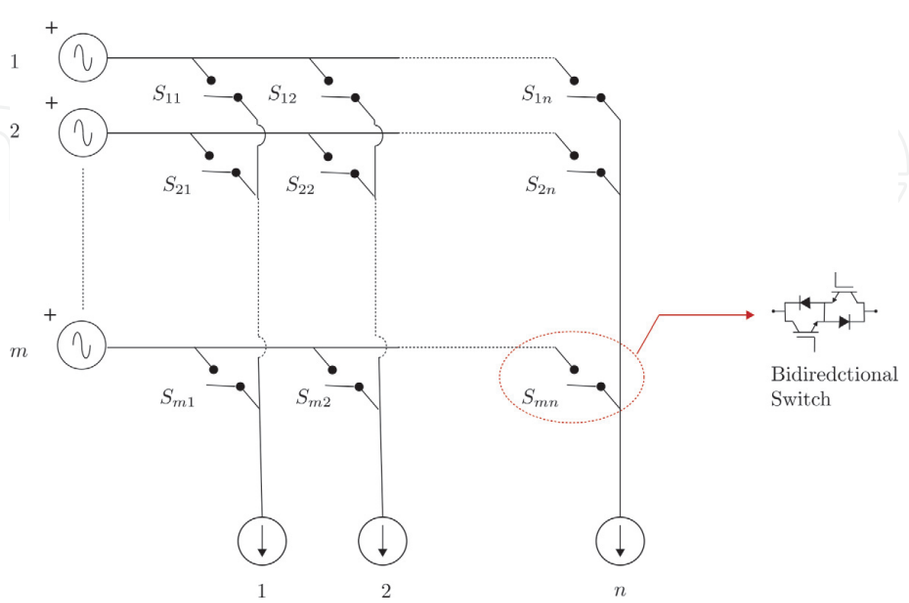

Figure 6.
mxn matrix converter equivalent model.

electrical shifting between each phase on a single three-phase group is still $2\pi/3$, constituting each individual symmetrical three-phase system.

Figure 6a shows a split-phase single-channel arrangement where the corresponding phase for each half-cell is derived as $y_{\ell}, y_{\ell+k}, y_{\ell+2k}$ with $\ell = [1, \ldots, k]$. A multichannel arrangement is shown in **Figure 6b**, which introduces some advantages, like full load dynamic decoupling and lower dc-link power rating. On the other hand, additional dc-link capacitors are required.

For both previously described topologies, SPWM is achieved by implementing the modulation as given in Eqs. (47) and (48) considering the asymmetry (if required) φ for each reference as $u^*_{xN}(\varphi)$.

In the case of space vector modulation for multiphase converters, it is necessary to extend the space vector representation into its corresponding subspaces. So as presented previously in this chapter, the output voltage space vector can be decomposed into $n/2$ orthogonal subspaces for n even and into $(n-1)/2$ orthogonal subspaces and single-dimensional quantity (common mode component) for n odd. Under this formulation, the reference voltage space vector to be synthesized can be expressed as in Eqs. (50) and (51) for n even and odd, respectively:

$$\boldsymbol{u}^*_{\boldsymbol{x}} = \left[u^{(1)}\, u^{(2)} \ldots, u^{(n)}\right]^T \tag{50}$$

$$\boldsymbol{u}^*_{\boldsymbol{x}} = \left[u^{(1)}\, u^{(2)} \ldots, u^{(n-1)}\right]^T \tag{51}$$

For each orthogonal subspace, there exits two active vectors, $\overline{v}_{uk}$ and $\overline{v}_{vk}$, corresponding to k orthogonal subspace. Each active vector is applied for a duty-cycle δ to synthesize the corresponding reference space vector, as in Eqs. (52) and (53):

$$\boldsymbol{u}^*_{\mathbf{x}} = \delta_{u1}\overline{v}^{(u1)} + \delta_{v1}\overline{v}^{(v2)} + \delta_{u2}\overline{v}^{(u2)} + \delta_{v2}\overline{v}^{(v2)} + \ldots + \delta_{u(n/2)}\overline{v}^{(u(n/2))} + \delta_{v(n/2)}\overline{v}^{(v(n/2))} \tag{52}$$

$$\boldsymbol{u}^*_{\mathbf{x}} = \sum_{j=1}^{n/2} \delta_{uj}\overline{v}^{(uj)} + \sum_{j=1}^{n/2} \delta_{vj}\overline{v}^{(vj)} \tag{53}$$

In the case of n odd, an additional degree of freedom is introduced by the common mode voltage v_{cm} which represents a single quantity and not a space vector as in Eq. (54):

$$\boldsymbol{u}^*_{\mathbf{x}} = \sum_{j=1}^{(n-1)/2} \delta_{uj}\overline{v}^{(uj)} + \sum_{j=1}^{(n-1)/2} \delta_{vj}\overline{v}^{(vj)} + \delta_{cm}v_{cm} \tag{54}$$

Eqs (53) and (54) can be interpreted as the partitioning of the $\alpha\beta$ stationary reference frame, into $n!$ or $(n-1)!$ adjacent sectors, and an additional common mode component, orthogonal to the $\alpha\beta$ subspace. Sector identification can then be achieved by implementing Eq. (55) where S corresponds to the given sector within the $\alpha\beta$ subspace:

$$S = \left(\frac{\theta}{M!}\right) + 1 \quad M = \begin{cases} n & \text{even number of subspaces.} \\ (n-1) & \text{odd number of subspaces.} \end{cases} \tag{55}$$

3.2 Matrix converter

The matrix converter is a direct AC-AC converter, which uses an arrangement of bidirectional switches, to connect each input phase, with a single corresponding output phase, thus generating an arrangement of *mxn* power switches, where *m* is the number of input phases and *n* the number of output phases. In **Figure 6,** the equivalent model of a *mxn* matrix converter is shown.

Due to the absence of a dc-link stage, the output voltages should be synthesized by selecting segments of the input voltages, by generating the adequate switching states. However, some switching state restrictions have to be taken into account, because of the particular topology of the matrix converter. Let's consider a generalized switching state S_{jk}, such that

$$S_{jk} = \begin{cases} 1 & \text{switch } S_{jk} \text{ is in on state.} \\ 0 & \text{switch } S_{jk} \text{ is in off state.} \end{cases} \qquad \forall j = 1, 2, \ldots, m \quad k = 1, 2, \ldots, n \tag{56}$$

For every instant t, the switching state S_{jk} must comply with both conditions stated in Eqs (57) and (58), thus meaning that for all t only one input phase is connected to one output phase, avoiding short-circuit condition, and also all output phases are connected to at least one input phase, ensuring no open-circuit condition. This last condition is intended to protect the bidirectional switches that cannot handle reverse current flow, due to the inductive energy discharge:

$$\sum_{j=1}^{n} S_{jk} = 1 \tag{57}$$

$$S_{jk} = 1 \quad \forall k = 1, 2, \ldots, n \tag{58}$$

Sinusoidal PWM scheme is implemented via the *Venturini* method [8], which is based on the solution of the relational input-output equations of the matrix converter, given in Eqs. (59)–(61):

$$[\boldsymbol{V_o}] = [M]\,[\boldsymbol{V_i}] \quad M = \begin{bmatrix} \delta_{11} & \delta_{12} & \ldots & \delta_{1m} \\ \delta_{21} & \delta_{22} & \ldots & \delta_{2m} \\ \vdots & \vdots & \ldots & \vdots \\ \delta_{n1} & \delta_{n2} & \ldots & \delta_{nm} \end{bmatrix} \tag{59}$$

$$[\boldsymbol{I_i}] = [M]^T\,[\boldsymbol{I_o}] \tag{60}$$

$$P_i = P_o \tag{61}$$

where $[\boldsymbol{V_o}]$ and $[\boldsymbol{V_i}]$ stand for the output and input voltage space vectors, respectively, $[\boldsymbol{I_o}]$ and $[\boldsymbol{I_i}]$ for the output and input current space vectors, $[M]$ is the low-frequency matrix or modulation index transfer matrix, and P_o and P_i correspond to the output and input active power.

On the other hand, space vector PWM formulation has no difference, as it is implemented in VSC. However, its complexity lies in the fact in that the absence of a nearly constant dc-link voltage, from which the reference voltage space vectors are synthesized. So both space vectors are to be composed using the input and output, voltage and current space vectors simultaneously. Moreover, the total number of possible switching states is $2^{(nm)}$, from which the forbidden conditions have to be considered. Space vector implementation is largely explained in literature [9].

The matrix converter has several advantages over multiphase voltage source converters, for multiphase drive applications. It is capable to synthesize nearly sinusoidal output voltage and currents, with low-order harmonics, thus improving the MMF distribution in machine air gap, eliminating torque ripple and preventing mechanical stresses on the output shaft. It provides bidirectional energy flow and provides full power factor control. Moreover, due to the absence of dc-link, it presents more power density, because of the lack of large capacitors, becoming an alternative for integrated drive converter configurations [10, 11]. However the complexity in the implementation of SPWM and SVPWM schemes, and the complex commutation strategy for the bidirectional switches, makes the matrix converter less attractive than the voltage source-based multiphase solutions.

There exist several variations of the direct matrix converter topology presented previously, such as the indirect and sparse matrix converter topologies, which are extensively described in literature [12]. These topological variations relay on the same basis but differ in the number and type of power switches used.

3.3 Nine-switch converter

The topology is derived from two three-phase voltage source converters that share a positive and a negative busbar, respectively, as shown in **Figure 7**.

The nine-switch converter has the ability to operate in back-to-back mode, as rectifier (A stage input) and inverter (B stage output), as two channel rectifier (A and B stages input) and as two stage inverter (A and B stages output), enabling the converter to handle a six-phase systems with just one channel, in spite of commonly 12-switch back-to-back topologies.

However, this topological advantage introduces some drawbacks to the nine-switch topology, because of the fact that S_x, S_y and S_z switches are shared by both converter stages A and B. Hence 3 switches are eliminated of the 12 needed for

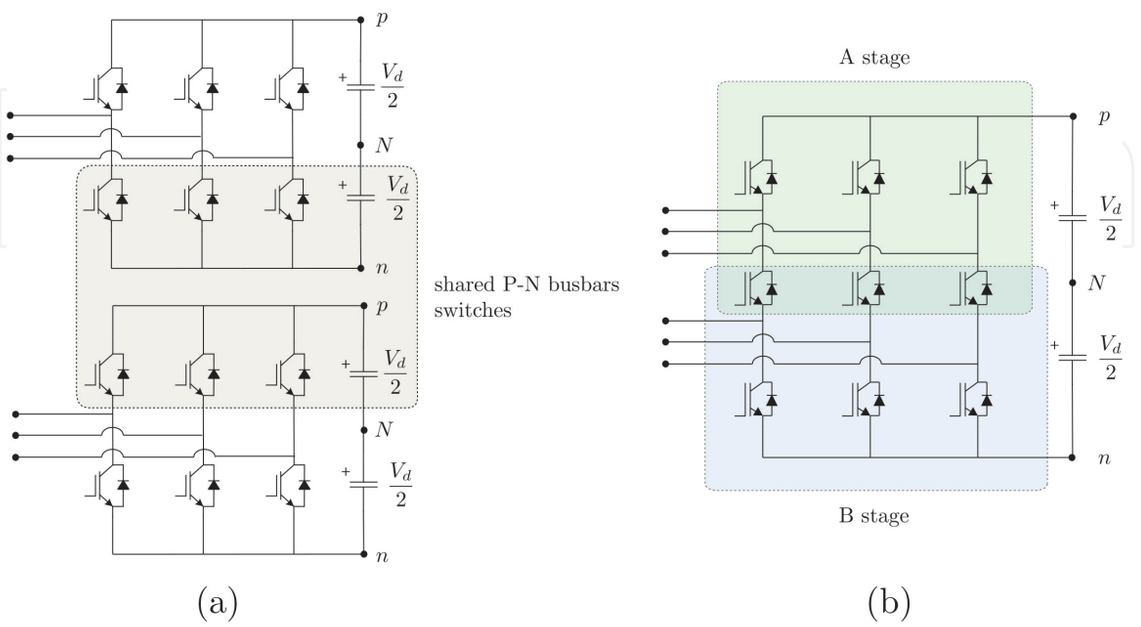

Figure 7.
(a) Classical arrangement with 12 switches. (b) Nine-switch converter topology.

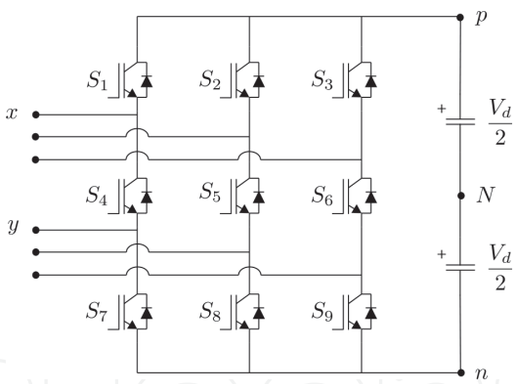

S_1	S_4	S_7	v_{xN}	v_{yN}
1	1	0	$V_d/2$	$V_d/2$
0	1	1	$-V_d/2$	$-V_d/2$
1	0	1	$V_d/2$	$-V_d/2$

Figure 8.
Nine-switch converter allowed switching states.

multiphase operation as in multichannel topology, some forbidden switching states are introduced, thus remaining 27 allowed states, and also the maximum output voltage gain is limited [13]. In **Figure 8,** the allowed switching states per leg are shown.

Carrier-based PWM modulation schemes such as sinusoidal PWM (SPWM), space vector modulation (SVM) and min-max (third harmonic injection) PWM [14] can be applied to the nine-switch converter, using two independent SPWM modulation schemes, one for each converter stage, as in the 12-switch back-to-back converter. However, because of the restrictions introduced to the modulation, pattern by the middle switches S_4, S_5 and S_6, its switching pattern can be obtained as in Eq. (62):

$$S_{k+3} = \overline{S_k \cdot S_{k+6}} \quad k = 1, \ldots, 3 \tag{62}$$

The implementation of SPWM considers the use of two voltage reference space vectors x^* and y^*, for each three-phase winding group. The NSC can operate either in constant (CFM) or variable frequency (VFM) modes, depending on each space vector angular frequency. However, due to the nature of the particular application in multiphase drives, the NSC is to be operated in the constant frequency mode, as presented in **Figure 9**.

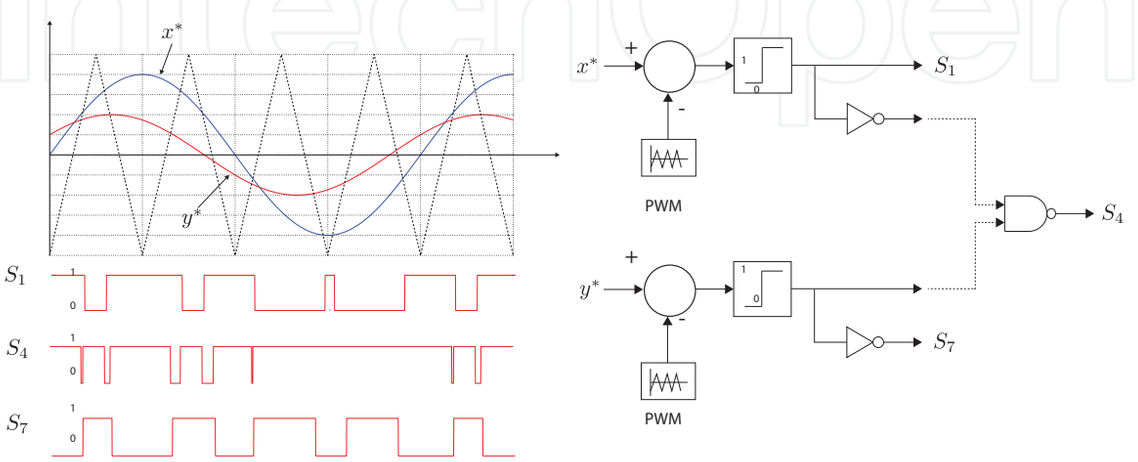

Figure 9.
CFM modulation.

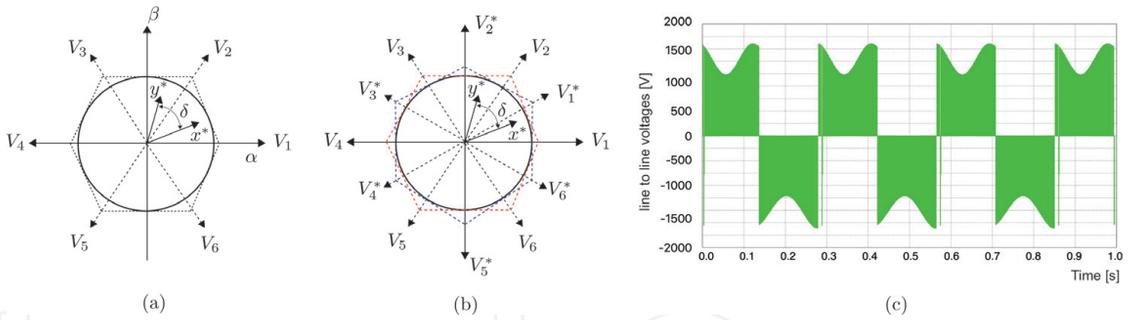

Figure 10.
Space vector decomposition. (a) Single carrier, (b) shifted multi-carrier and (c) line-line voltage.

For the constant frequency mode operation (CFM), both reference space vectors x^* and y^* have the same angular frequency ω_k, preserving its spatial shifting δ, so they are to be found at least in contiguous sectors of the voltage hexagon, as shown in **Figure 10a**, being the maximum voltage gain g given in Eq. (63):

$$g = \frac{1}{\sqrt{3}\left(\frac{\delta}{2} + \frac{\pi}{3}\right)} \tag{63}$$

By introducing a phase shifting of $\pi/6$ between both PWM carriers, a second group of active vectors is introduced as shown in **Figure 10b**, which results in a voltage gain as in Eq. (64):

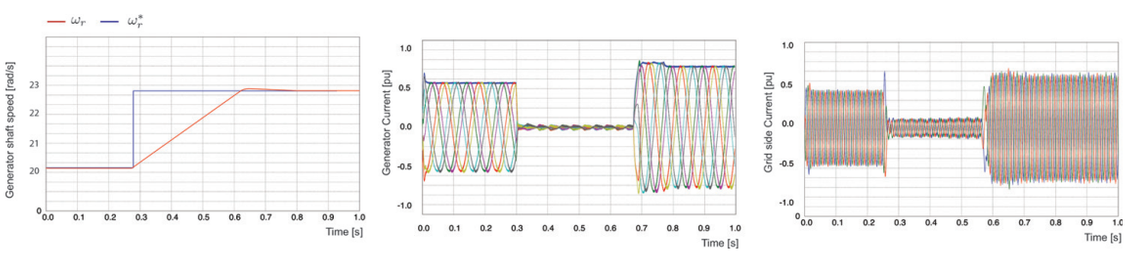

Figure 11.
Simulation results for a back-to-back NSC for wind energy conversion.

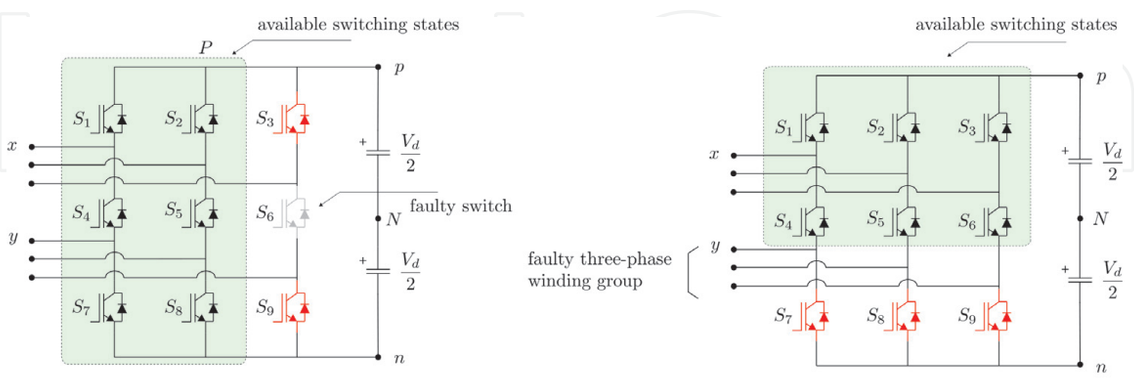

S_2	S_5	S_8	v_{xN}	v_{yN}	v_{pN}	v_{qN}
1	1	0	$V_d/2$	$-V_d/2$	$V_d/2$	$V_d/2$
0	1	1	$V_d/2$	$-V_d/2$	$-V_d/2$	$-V_d/2$
1	0	1	$V_d/2$	$-V_d/2$	$V_d/2$	$-V_d/2$

S_1	S_4	S_7	v_{xN}	v_{yN}
0	1	1	$-V_d/2$	$-V_d/2$
1	0	1	$V_d/2$	$-V_d/2$

Figure 12.
Nine-switch converter reconfiguration under faulty operation.

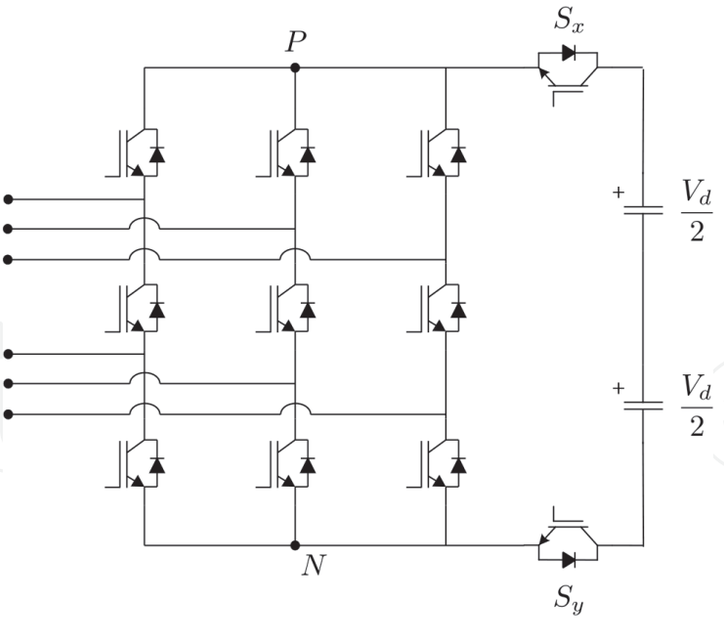

Figure 13.
11-switch converter.

$$g = \frac{1}{\sqrt{3}\left(\delta + \frac{\pi}{6}\right)} \tag{64}$$

Recently, the NSC has been gaining much attention in various applications like isolated wind-hydro hybrid power system, power quality enhancement and hybrid electric vehicles because of its ability to interconnect multiphase power systems in common or split configurations and also independent three-phase-based systems, in constant or variable frequency modes. **Figure 11** shows simulation results for a wind energy conversion system (WECS) based on a nine-switch back-to-back converter topology [15].

Another important feature of the NSC is the capability to rearrange its switching states under single- or multiple-switch faulty conditions [16], as shown in **Figure 12**.

3.4 11-switch converter

The 11-switch converter, presented in [17], consists of a modified topology of the 9-switch converter topology, previously discussed. As shown in **Figure 13**, this topology introduces two additional switches S_x, S_y, whose main propose is to mitigate the common mode voltage during the zero switching states.

4. Control of multiphase electric drives

As discussed previously in this chapter, the electromechanical torque developed by the multiphase machine depends only on the state variables in $\alpha\beta$ subspace, thus meaning that the other subspaces do not contribute to the energy conversion process but only losses. This fact makes possible the implementation of oriented control schemes, such as field-oriented control (FOC), direct torque control (DTC) and model-based predictive control (MBPC), in a synchronous reference frame dq, by rotating the state variables in $\alpha\beta$ subspace.

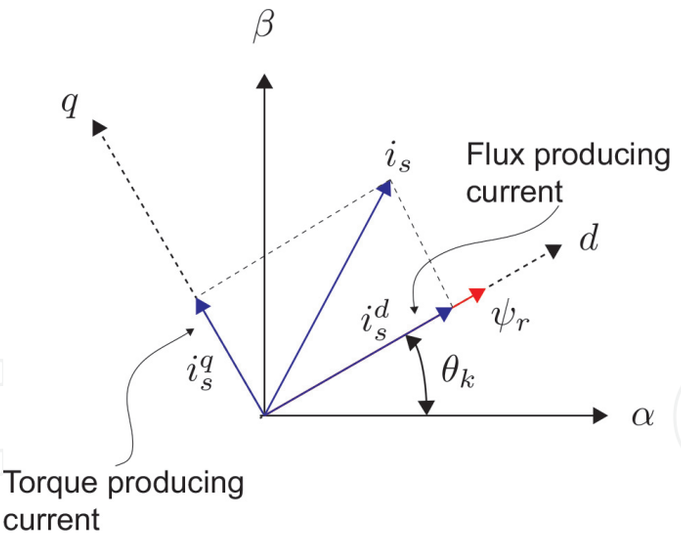

Figure 14.
dq synchronous reference frame rotation.

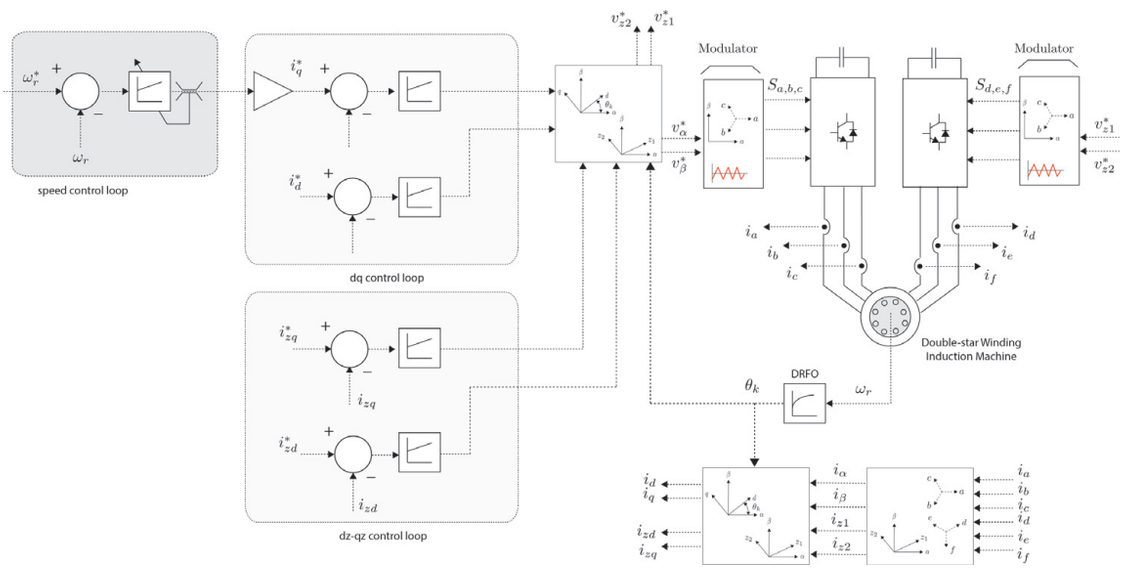

Figure 15.
Field-oriented control scheme of a dual three-phase winding induction machine.

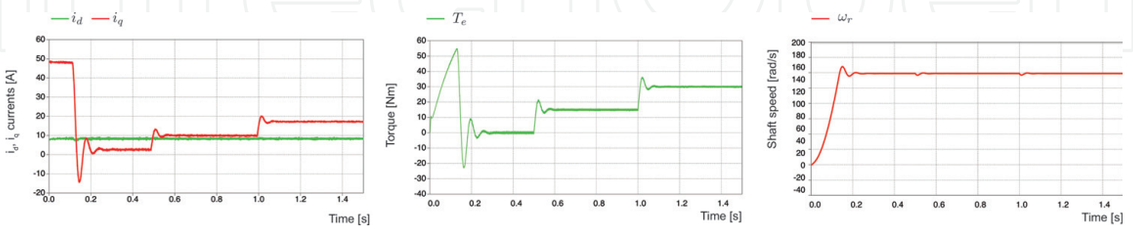

Figure 16.
Dual three-phase winding induction machine FOC scheme simulation results.

An additional control loop in the *dq* reference frame can be implemented, to compensate the losses in the remaining subspaces. Control goals for the multiphase drive can be summarized as maximum torque per Ampere operation, control of nominal flux and control of rotor speed/torque.

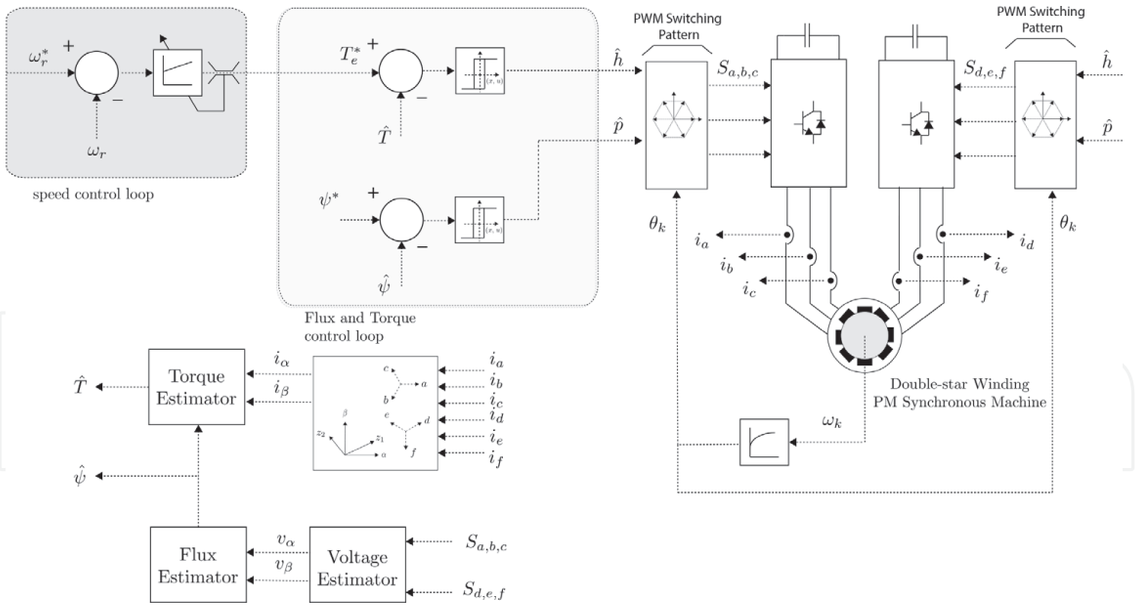

Figure 17.
Direct torque control scheme of a dual three-phase winding PM synchronous machine.

4.1 Field-oriented control

The characteristics of field-oriented control (FOC) have made this control strategy the most widely used for high-demanding industrial applications. Field-oriented control is based in the decoupling of the current space vector, into a flux-producing component and a torque-producing component. This is achieved by rotating the current space vector from $\alpha\beta$ subspace, into the synchronous rotating reference frame dq, oriented with respect to the rotor flux linkage space vector, as shown in **Figure 14**.

In this way the magnetizing flux can be controlled, so that the machine operates with nominal flux under any condition, and also torque can be controlled only by i_s^q, because $\psi_r^q = 0$, due to the orientation of ψ_r which only exists in the direct axis orientation. Implementation of the FOC scheme for a multiphase AC drive is shown in **Figure 15**.

Figure 16 shows simulation results for a dual three-phase induction machine drive using FOC scheme, under load impact.

The main drawbacks of FOC are the requirement in the estimation of the rotor flux linkage space vector and the rotation of the state space variables into this synchronous reference frame, becoming a very complex process. Also, as the dynamic response, this control strategy is limited by maximum bandwidth achievable for the PI controllers, which represents one of the fundamental limitations of linear controllers.

4.2 Direct torque control

Direct torque control (DTC) is based on the estimation of torque and flux directly from the state variables of the AC machine. The torque and flux can be controlled by applying the suitable voltage vector, synthesized by the available switching states of the converter.

The required voltage vector is chosen via a switching table, as function of the actuation of the torque and flux loop hysteresis controllers (in terms of increasing or decreasing flux or torque for a certain operational point). Implementation of the DTC scheme for a multiphase AC drive is shown in **Figure 17**.

The main characteristics of DTC are its simple implementation and a fast dynamic response achieved by using hysteresis controllers. Furthermore, the required switching states are directly assigned from the switching table algorithm, so no modulator is needed.

5. Conclusions

In this chapter, the main advantages of multiphase machine drives for its application in high-demanding industrial processes, traction and renewable energy grid interfacing were presented, with their main focus on multiphase power converter topologies. Various technical issues related to classical multiphase converters, based on multicell arrangements, were discussed, as well as some new converter topologies, such as the nine-switch converter (NSC) and 11-switch converter (ESC), were introduced.

The main advantages of classical multiphase converter topologies, based on voltage source converters (VSC), are mostly referred to their topological simplicity and their capability to implement conventional sinusoidal-PWM-based techniques. On the other hand, the increasing number of semi-conductors and dc-link capacitors (in the case of multichannel arrangements) and the need for common mode current compensation are their major drawbacks. In this field of application, matrix converters arise as suitable alternative, which enables the possibility to handle multiple output phases. However, maximum voltage gain limitations and the complexity of the modulation and commutation strategies are their main disadvantages, when compared to classical topologies.

Nine-switch and eleven-switch converters appear as a middle-point alternative between multicell and matrix converter topologies. These topologies allow the use of sinusoidal-PWM-based modulation techniques, without the need of complex modulation and commutation strategies (as in the case of the matrix converter), using a single dc-link stage.

Implementation of control strategies for multiphase drive, such as field-oriented control (FOC) and direct torque control (DTC), has been easily achieved by using multi-space decomposition of the each state space vectors (representing a state space variable).

Author details

Carlos A. Reusser
Department of Electronics, Universidad Tecnica Federico Santa Maria, Valparaiso, Chile

*Address all correspondence to: carlos.reusser@usm.cl

References

[1] Levi E. Multiphase electric machines for variable-speed applications. IEEE Transactions on Industrial Electronics. 2008;**55**(5):1893-1909

[2] Levi E. Advances in converter control and innovative exploitation of additional degrees of freedom for multiphase machines. IEEE Transactions on Industrial Electronics. 2016;**63**(1):433-448

[3] Zhang Z, Matveev A, Ovrebo S, Nilssen R, Nysveen A. State of the art in generator technology for offshore wind energy conversion systems. In: Electric Machines Drives Conference (IEMDC), 2011 IEEE International; May 2011. pp. 1131-1136

[4] Li H, Chen Z. Design optimization and evaluation of different wind generator systems. In: International Conference on Electrical Machines and Systems, 2008. ICEMS 2008; Oct 2008. pp. 2396-2401

[5] Levi E, Bojoi R, Profumo F, Toliyat HA, Williamson S. Multiphase induction motor drives—A technology status review. IET Electric Power Applications. 2007;**1**(4):489-516

[6] Banerjee A, Tomovich MS, Leeb SB, Kirtley JL. Control architecture for a doubly-fed induction machine propulsion drive. In: 2013 Twenty-Eighth Annual IEEE Applied Power Electronics Conference and Exposition (APEC); March 2013. pp. 1522-1529

[7] Leon JI, Kouro S, Franquelo LG, Rodriguez J, Wu B. The essential role and the continuous evolution of modulation techniques for voltage-source inverters in the past, present, and future power electronics. IEEE Transactions on Industrial Electronics. 2016;**63**(5):2688-2701

[8] Venturini M, Alesina A. The generalised transformer: A new bidirectional, sinusoidal wave- form frequency converter with continuously adjustable input power factor. In: 1980 IEEE Power Electronics Specialists Conference; June 1980. pp. 242-252

[9] Lee MY, Wheeler P, Klumpner C. Space-vector modulated multilevel matrix converter. IEEE Transactions on Industrial Electronics. 2010;**57**(10): 3385-3394

[10] Wheeler PW, Clare JC, Apap M, Lampard D, Pickering SJ, Bradley KJ, et al. An integrated 30kw matrix converter based induction motor drive. In: 2005 IEEE 36th Power Electronics Specialists Conference; June 2005. pp. 2390-2395

[11] Abebe R, Vakil G, Calzo GL, Cox T, Lambert S, Johnson M, et al. Integrated motor drives: State of the art and future trends. IET Electric Power Applications. 2016;**10**(8):757-771

[12] Pena R, Cardenas R, Reyes E, Clare J, Wheeler P. A topology for multiple generation system with doubly fed induction machines and indirect matrix converter. IEEE Transactions on Industrial Electronics. 2009;**56**(10): 4181-4193

[13] Liu C, Wu B, Zargari N, Xu D, Wang J. A novel three-phase three-leg ac/ac converter using nine igbts. IEEE Transactions on Power Electronics. 2009;**24**(5):1151-1160

[14] Hava A, Kerkman R, Lipo T. Simple analytical and graphical tools for carrier based pwm methods. In: Power Electronics Specialists Conference, 1997. PESC '97 Record, 28th Annual IEEE, Vol. 2; Jun 1997. pp. 1462-1471

[15] Reusser CA, Kouro S, Cardenas R. Dual three-phase pmsg based wind energy conversion system using 9-switch dual converter. In: 2015 IEEE Energy Conversion Congress and Exposition (ECCE); Sep. 2015. pp. 1021-1022

[16] Reusser CA. Full-electric ship propulsion, based on a dual nine-switch inverter topology for dual three-phase induction motor drive. In: 2016 IEEE Transportation Electrification Conference and Expo (ITEC); June 2016. pp. 1-6

[17] Kumar EA, Satyanarayanat G. An eleven-switch inverter topology supplying two loads for common-mode voltage mitigation. In: 2017 IEEE PES Asia-Pacific Power and Energy Engineering Conference (APPEEC); Nov 2017. pp. 1-6